ELSEVIER

Biophysical Chemistry 114 (2005) 137–147

Biophysical Chemistry

http://www.elsevier.com/locate/biophyschem

Structural studies of the biomineralized species of calcified pancreatic stones in patients suffering from chronic pancreatitis

K.V. Narasimhulu[a,1], N.O. Gopal[a], J. Lakshmana Rao[a,*], N. Vijayalakshmi[b], S. Natarajan[b], R. Surendran[c], V. Mohan[c]

[a]*Department of Physics, Sri Venkateswara University, Tirupati-517 502, India*
[b]*Department of Physics, Madurai Kamaraj University, Madurai-625 021, India*
[c]*Department of Surgical Gastroenterology, Government Stanley Medical College, Chennai-600 001, India*
[d]*Madras Diabetes Research Foundation, Chennai-600 086, India*

Received 9 July 2003; received in revised form 5 November 2004; accepted 22 November 2004
Available online 15 December 2004

Abstract

The pancreatic stones (*Pancreatic calculi*) collected from patients suffering from chronic calcific pancreatitis were studied in a view to explore the constituents involved in the calcification. The calcified stones were characterized by XRD, EPR and IR spectroscopic techniques. The detailed studies indicate that these stones consist of calcium carbonate as a major component, besides phosphates and other protein content. The presence of aragonite phases in the biomineralized stones is also discussed. The EPR spectra gave an evidence of the presence of traces of manganese in different oxidation states, which is used as one of the EPR probes in the present work. The samples were sintered at different temperatures to remove all the organic matter, and their EPR spectra have been studied to obtain detailed information regarding the changes in the symmetry of these stone samples. The X-irradiated sample was also characterized by EPR and the resonance signals are attributed to freely rotating CO_2^- radicals. The infrared spectrum reveals the presence of many organic bands corresponding to the protein amides.

Keywords: Pancreatic stones; Calcification; Pancreas; EPR; Thermal treatment; X-irradiation; Infrared spectra

1. Introduction

The pancreas in all mammalian species is an important gland located in the upper abdomen behind and below the stomach. The pancreas has both exocrine and endocrine functions. The endocrine part of the pancreas consists of the islets of Langerhans, which have alpha, beta and delta cells, which secrete glucagons, insulin and stomatostatin, respectively [1]. The exocrine part of the pancreas is concerned with digestion as it secrets several digestive enzymes [1]. Inflammation of the pancreas is known as pancreatitis and may be classified as acute and chronic pancreatitis. Chronic pancreatitis is a continuing inflammatory disease of the pancreas characterized by irreversible morphological changes that typically causes pain and permanent loss of pancreatic function. In the natural history of pancreatitis, intractable pain dominates other clinical complications, calcification sets in soon after pain leading to stone formation (*Pancreatic calculi*) in the main duct [1,2]. Biological fluids are generally supersaturated with respect to calcium salts such as oxalates in urine, phosphates in saliva, and carbonates in bile or pancreatic juice. It might become harmful if continuous crystal growth is allowed, leading to the formation of stones. Inhibition of stones is mainly done by protein inhibitors. In the pancreas, the stone formation is inhibited by a 144 amino acid glycoprotein (15.5 kDa) showing structural homology with C-type lectins and synthesized by pancreatic acinar cells [3]. However, the role of the pancreatic stone protein (PSP), lithostathine, is controversial and is expected to contribute to the stone formation [4].

* Corresponding author. Fax: +91 877 2248499.
E-mail address: jlrao46@yahoo.co.in (J.L. Rao).
[1] Present address: Department of Chemistry, National Taiwan University, Taipei 106, Taiwan, ROC.

0301-4622/$ - see front matter © 2004 Elsevier B.V. All rights reserved.
doi:10.1016/j.bpc.2004.11.013

In south India, the commonest cause of *pancreatic calculi* is tropical chronic pancreatitis [5,6]. This long-standing disease very often affects the endocrine function of the pancreas resulting in diabetes. This form of diabetes, which occurs due to tropical chronic pancreatitis, is called Fibrocalculous Pancreatic Diabetes (FCPD) [5,6]. Pancreatic concretions are pure white or yellowish in color, spherical, cuboidal or cylindrical in shape; multiple in number and hard in consistency [2]. Studies on the composition of *P. calculi* using X-ray diffraction revealed calcium carbonate as the primary constituent [2,7]. In addition, traces of nickel and fatty acids, organic matrix with desquamated epithelium, fibrin, mucoid substances and protein have also been reported [2]. Pancreatic stones specifically contain a 15.5 kDa protein called lithostathine, also called pancreatic stone protein, inhibiting the calcite growth and tightly binds $CaCO_3$ crystals modifying the crystal habit in vitro [8]. It is known that the pancreas is one of the most sophisticated organs for the protein synthesis, secretion and electrolyte exchange, all of which require large amount of energy and oxygen. Therefore, constitution expression of Mn-SOD in the pancreas may serve as a biochemical defense against oxidation of cellular constituents by free radicals that escape the electron transport system [9]. It has later been proven in several cases, particularly related to diseases of human pancreas, where the cytoplasmic values of Mn-SOD were decreased in pancreatic cells from chronic pancreatitis specimen when compared to normal pancreas [10].

EPR and electronic spectral techniques have been extensively used in studying many biological systems containing transition metal ions and/or the free radicals as such. In this direction, recent works on EPR, infrared and other spectroscopic studies have extensively been carried out in a variety of biological systems [11–15]. In particular, a study on the binding of Mn^{2+} to bovine pancreatic deoxyribonuclease I and DNA was studied by Jouve et al. using EPR technique [11]. They clearly demonstrated that Mn^{2+} binds to DNA and the Ca^{2+} clearly competes with two strong Mn^{2+} sites, which are inequivalent by nature. They also indicated the Mn^{2+} binding to the phosphate groups in bovine pancreatic DNase. In the present work, the authors have made an attempt to study the calcified stones of *pancreatic calculi* samples in human suffering from chronic pancreatitis. The study is undertaken, assuming the fact that there are many factors that influence the calcification including the protein, organic solvents, etc. The present study explores the structure and possibility of involvement of various components in calcification using X-ray diffraction, IR and EPR spectroscopy. In particular, the EPR spectra have been studied at various temperatures to study the novel information connected with the structure and compositional details of the biomineralized *pancreatic calculi*.

2. Experimental

The pancreatic calculi samples were collected from Dr. Mohan's M.V. Diabetes Specialities Centre and The Madras Diabetic Research Foundation, Chennai, India. These samples were dried at room temperature first and then stored at room temperature in a desiccator. The heat treatments for the same were given through controlled temperature furnaces with an accuracy of ± 2 °C. The samples for XRD were simply ground into a fine powder using a clean agate mortar and pestle. The X-ray powder diffractograms of the powdered samples of the *pancreatic calculi* were recorded using a computer controlled Siemens X-ray powder diffractometer with Cu-Kα X-radiation of wavelength 1.5418 Å. For the EPR spectral measurements, the samples were dried and ground thoroughly in a tested clean agate mortar into a fine powder. About 100 mg of the fine powder was taken into fresh quartz tubes of EPR grade and were inserted into the cylindrical cavity (TEO_{11}). The EPR spectra were recorded on a JEOL FE1X ESR spectrometer operating at X-band microwave frequency equipped with TE_{011} cylindrical cavity with 100 kHz field modulation. The temperature variation EPR studies were performed from 123 to 295 K by using JES UCT 2AX variable temperature controller. For thermal sintering of the samples, ultra pure silica crucibles were used for the entire experiments. The Infrared spectral studies were performed in transmission mode on a JASCO FTIR spectrophotometer using KBr pellet technique in conventional method.

3. Results

The XRD recorded for one of the samples of *pancreatic calculi* is shown in Fig. 1. All the samples were identified as calcium carbonate stones. By comparing the location of the peaks in the XRD with the JCPDS data on inorganic compounds, the peaks were identified as due to both calcium carbonate and the calcium phosphate, with calcium carbonate (in calcitic form) as major component as evidenced from the intense peak (104) of calcium carbonate. The other peaks corresponding to calcite, aragonite and minor components of phosphates are indexed in the XRD picture shown in Fig. 1. The dimorphic form of $CaCO_3$ in the presence of protein matrix is in good agreement with that observed for other systems in the presence of soluble proteins [16,17]. No other phases in any form are observed other than the reported ones, as the X-ray diffraction data is scanned in broad range.

The mechanism of calcite crystal growth inhibition by N-terminus undecapeptide of lithostathine, a crystal growth inhibitor has been well studied by Gerbaud et al. [15]. In their study, it was reported that the human lithostathine modifies the crystal habit of calcite from rhombohedral $[10\hat{1}4]$ usual habit to needle like habit through [1120] crystal form. However, the increase in calcification decreases the lithostathine secretion leading to chronic

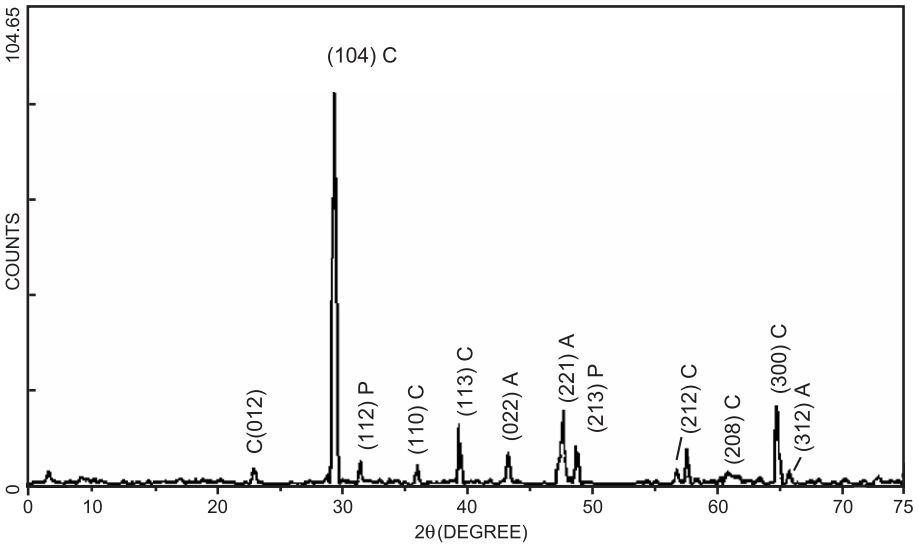

Fig. 1. X-ray diffraction pattern of *P. calculi* sample. The peaks are indexed in view of the presence of both calcite (C) and aragonite (A) phases. The peaks correspond to minor compositions of phosphates of calcium (P) are also seen in the figure.

pancreatitis disease. The EPR spectra of polycrystalline *P. calculi* show no significant EPR signals. However, when the modulation is increased weak EPR signals are observed. Fig. 2 shows the typical EPR spectrum of fresh *P. calculi* sample at room temperature. The room temperature EPR spectrum exhibits weak six-line hyperfine spectrum centered at g=1.9964 characteristic of Mn^{2+} ions with isotropic hyperfine structure arising from the central transition $|-1/2\rangle \leftrightarrow |+1/2\rangle$ of Mn^{2+} ion with electron spin S=5/2 and nuclear spin I=5/2. In-between these allowed hyperfine lines, the forbidden lines ($\Delta M_I \neq 0$) as doublets are also observed. The observed EPR spectra are well comparable with the Mn^{2+} in Ca-environments in literature [17–20].

The observed EPR spectrum can be explained by the spin-Hamiltonian of the form [21]

$$\mathcal{H} = \beta B g S + D\left(S_z^2 - S(S+1)/3\right) + E\left(S_x^2 - S_y^2\right) + S\hat{A}I \quad (1)$$

where the first term represents the electron-Zeeman interaction, the second and third terms represent the zero-field contribution and the fourth term represents the hyperfine interaction.

The hyperfine splitting constant A can be calculated from the position of the allowed hyperfine lines using the formula [22]

$$B_m = B_0 - AM_I - A^2/8B_0\left(I(I+1) - 4M_I^2\right) \quad (2)$$

where B_m is the magnetic field corresponding to M_I hyperfine line. B_0 is the resonance magnetic field, $B_0 = h\nu/g_0\beta$, g_0 is the isotropic g-factor. A is the isotropic hyperfine splitting parameter and M_I=−5/2, −3/2, −1/2, 1/2, 3/2, 5/2. The hyperfine splitting parameter is found to be A=89±2 G.

From the observed forbidden doublet lines, the zero-field splitting parameter D, has been calculated by using the formula [22]

$$\Delta B = \left(2D^2/B_m\right)\left[1 + 16\left(B_m - 8AM_I\right)^2 \Big/ 9B_iB_m - 64AM_I\right] \quad (3)$$

where $B_m = B_0 - AM_I - \{I(I+1) - M_I^2\}A^2/2B_0$.

Here I, M_I and B_0 are the nuclear spin, nuclear magnetic quantum number and the resonance magnetic field, respec-

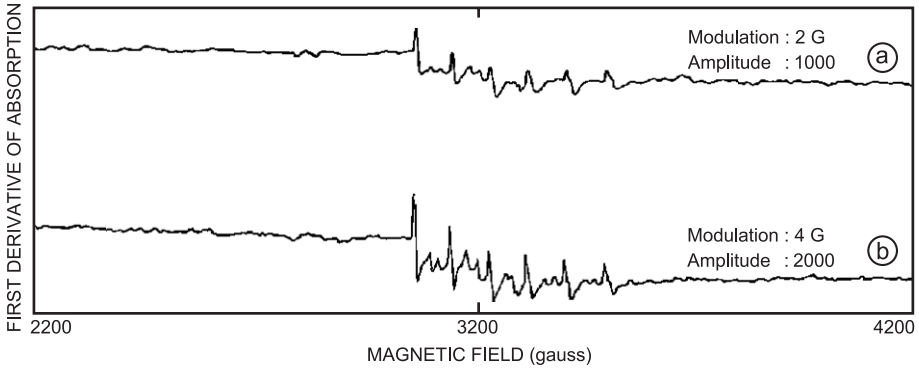

Fig. 2. EPR spectrum of fresh *P. calculi* stone sample at room temperature with different instrumental parameters.

Table 1
Spin-Hamiltonian parameters for Mn^{2+} ions in different polycrystalline systems of Ca-lattices for comparison

System	g-Values	A (G)	D (G)	Reference
(1) *P. calculi* (RT)	1.9964	89	−125	Present work
(2) *Mytilus* sp. Nacre (Aragonite)	1.999	85	−154	[19]
(3) Marine shell $CaCO_3$ (heat treated calcite)	1.998	89	−96	[20]
(4) *Pila globosa* sp.[a]	2.010	91	125	[20]
(5) CaS	2.0015	72	–	[40]

[a] Major component is calcite, but still has minor concentrations of aragonite in it, as evidenced by IR and EPR.

tively. B_i is the observed magnetic field position of each allowed hyperfine line and the other symbols have their usual meaning.

The g and A parameters have been calculated and are compared with other systems as given in Table 1. A clear examination of the zero-field splitting parameter D in the EPR spectrum reflects the extent to which the coordination sphere of Mn^{2+} deviates from perfect cubic symmetry or the symmetry possessed by the material on complex formation. In evaluating the zero-field splitting parameter (D), we considered the sign of the hyperfine splitting constant (A) as negative since for Mn^{2+} ions, the A value is always negative [19]. The magnitude of zero-field splitting parameter D obtained in the present work is 125 G and is in good agreement with that reported for polycrystalline $CaCO_3$ systems where calcite is found to be a major component [19,20]. The sign of D value is relative and can be known from the hyperfine separations of the spectral lines. As the EPR spectrum recorded is polycrystalline one, it is difficult to determine the same in this work. However, there are a number of reports in literature [19,20,22], where the negative sign was assigned for the D value. Hence, the sign of D is assumed to be negative in the present case. These values agree well with those reported for biomineralized, calcified species containing both aragonite and calcite reported in literature [19,20].

The *P. calculi* may contain many salts of calcium, like carbonate, phosphate and organic matter along with protein content. When the metal ion is strongly bound to the protein/enzyme, it is always difficult to find the paramagnetic state of bind metal ions to protein sites, where there is no free paramagnetic sites [11] at room temperatures. In order to exploit the same, the sample was heated at different temperatures. Hence, the sample has been sintered at different temperatures 400, 600 and 700 °C and its EPR spectral response has been studied. This enables one to study the changes in the environment around the metal ion and release of free metal ions from the binding sites with temperature.

3.1. The effect of thermal sintering on the EPR spectra of P. calculi

In order to know the exact inorganic matter associated with the pancreatic stone calcification, the calculi was sintered at different temperatures, for about 2–3 h in air. The sintering of the sample at 100 °C or below did not show any difference in the EPR spectral features. When the sample is sintered above 200 °C, a new sharp line appears at g=2.0000 with a linewidth of about 8 G, but no appreciable change is observed in the hyperfine spectra of Mn^{2+} ions. When the sample is heated further to 400 °C, the intensity of this free radical signal increases as shown in Fig. 3. This free radical signal may be due to the CO_3^- radical, which is observed in many carbonate lattices [23–25], even at room temperature.

In the sample of *P. calculi* sintered at 400 °C, a clear change is observed in the EPR spectra. A new set of sextet hyperfine lines of Mn^{2+} has been observed as shown in Fig.

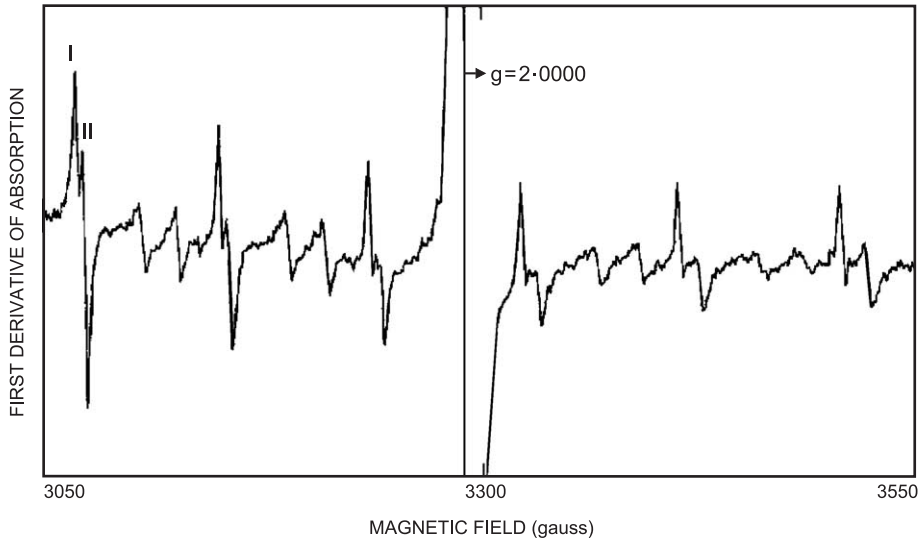

Fig. 3. EPR spectrum of *P. calculi* sample sintered at 400 °C showing two sites of Mn^{2+} ions clearly.

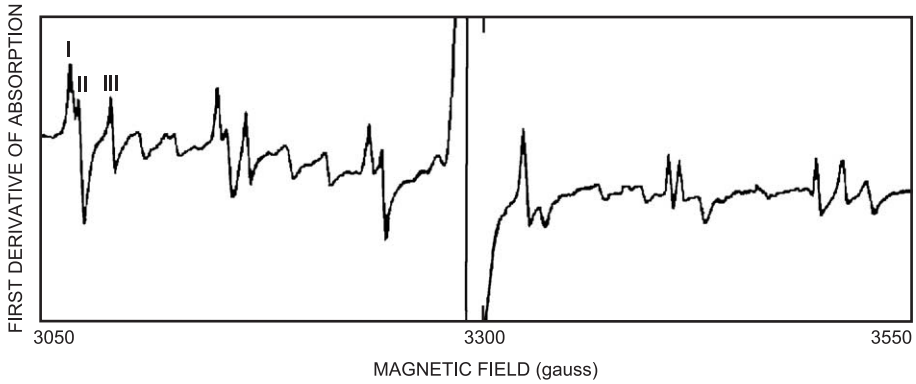

Fig. 4. EPR spectrum of *P. calculi* sample sintered at 600 °C showing three sites of Mn^{2+} formed due to cationic vacancy created by PO_4^{3-}.

3 and the intensity of the resonance signal at g=2.0 (free radical) increases considerably. This change, however, is unusual in the earlier studies of Ca-hosts [19,20] where a simple spectrum or an unchanged spectrum of Mn^{2+} ions was seen at a similar case. This may lead to a possibility that the composition of the present sample differs from the naturally occurring Ca-host materials studied in literature. If the sintering temperature of the *P. calculi* sample is further increased, one more set of additional lines is seen at 600 °C as shown in Fig. 4. The total hyperfine lines sums up to three sets which clearly contain the forbidden doublet lines also and are usually observed for Mn^{2+} ions in crystalline materials. The appearance of additional set of sextet hyperfine EPR lines corresponding to Mn^{2+} ions in this sample may be due to the presence of phosphate material in significant concentration comparable with the carbonate content which will be discussed in next section. At about 650 °C, the free radical signal completely vanishes and the new set of lines is clearly seen even after 650 °C.

At a sintering temperature of about 700 °C, only one set of hyperfine lines characteristic of a single site of Mn^{2+} ions were noticed as shown in Fig. 5. The disappearance of the free radical signal is followed by the presence of a weak signal centered at g=1.9983. A significant intense four line set is also observed as is marked in Fig. 5, which is more unusual. This can be assigned to various isotopic forms of chromium (^{54}Cr, ^{53}Cr, ^{52}Cr, ^{50}Cr). A novel biological role of chromium in regulation of insulin function was described [26]. Conditions that increase circulating glucose and insulin concentrations increase urinary chromium output [27].

The EPR spectra revealed the presence of different sites present at different experimental conditions of the sample. From the EPR spectra measured so far at different sintering temperatures, the spin-Hamiltonian parameters and zero-field splitting parameters of which will describe the oxidation state and the symmetry information of the Mn^{2+} ions in *P. calculi* sample are given in Table 2. Temperature variation EPR studies have been performed (for the sample sintered at 700 °C) in the range 123 to 295 K. Not much variation is observed in the line widths of the sextet hyperfine lines. However, the intensity of the spectral lines increases with decreasing temperature following usual Boltzmann law. In the EPR spectrum recorded below 213 K, a few more weak resonance signals are observed at g=2.1850, 2.4510 and 2.7431 and are shown in Fig. 6. Besides these, two more resonance lines at g=3.1970 and 4.0570 have also been observed but are not shown in Fig. 6, within the field covered. The signals, which lie between

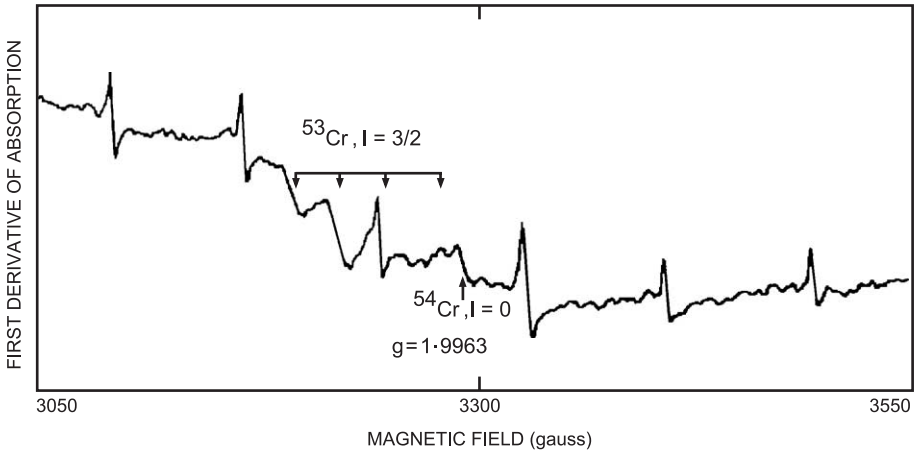

Fig. 5. EPR spectrum of *P. calculi* sintered at 700 °C. Note clearly the absence of free radical signal and the presence of the signals due to ^{54}Cr, ^{52}Cr, ^{50}Cr. The quartet hf lines marked in the figure are due to ^{53}Cr with I=3/2.

Table 2
The spin-Hamiltonian and zero-field splitting parameters of Mn^{2+} ions in *P. calculi* sample at different sintering temperatures

Temperature (°C)	Site	g	D (G)	A (G)
400	I	2.0028	125	89
	II	1.9970	125	90
600	I	2.0034	113	83
	II	1.9973	113	84
	III	1.9873	114	88
700		1.9960		82

The errors in g, A and D values are ±0.0005, ±2 G and ±5 G, respectively.

$3.2>g_{eff}>2.4$, are generally more evident at low temperatures. They appear with temperature dependent line widths and the line shapes may arise probably due to those systems having $S>1/2$. By thorough comparison, one can safely affirm that these may be due to Mn^{4+} ions with $S=3/2$ [28]. The resonance signal observed at $g=4.0570$ is due to Mn^{2+} ions, and the resonance signals at $g=3.1970$, 2.7431, 2.4510 and 2.1850 are not only due to Mn^{2+} ions but also due to presence of Mn^{4+} ions in a low symmetry environment [29,30]. The sextet hyperfine lines of Mn^{2+} ions centered at $g=1.9964$ corresponding to $\Delta M_s=1/2\leftrightarrow-1/2$ transition have also been seen in this spectrum clearly.

3.2. Effect of X-irradiation on the P. calculi samples as monitored by EPR

The samples have also been subjected to X-irradiation for 5 h. The EPR spectra of these irradiated samples show marked effect over the un-irradiated ones. It can be noted that the changes in EPR spectral patterns have been seen in the free radical region as is shown in Fig. 7. These samples were not subjected to any thermal effects at any stage. The strong peak centered at $g=1.9990$ is overlapped with other signals; however, the other signals may also be seen easily. Similar observations have also been reported in the case of some carbonate materials irradiated with gamma rays [24,25,31]. The signals centered at $g=2.0083$, 2.0022, 1.9998, 1.9968 and 1.9944 observed after X-irradiation are the characteristic peaks of free radical, CO_2^- ion which will be discussed in the next section.

3.3. Infrared spectral studies

The infrared spectral studies have been performed on the *P. calculi* material. It is known that *P. calculi* stones may contain carbonates, phosphates and other salts of calcium. The infrared spectrum of *P. calculi* recorded at room temperature is shown in Fig. 8. The observed bands at 3433 cm^{-1} can be attributed to the OH bands of the carboxylic group or the residual water. The bands between 2933 and 2863 cm^{-1} are due to C–H stretching vibrations. These bands are strong and the splitting of the triply degenerate band around 2863 cm^{-1} corresponds to the symmetric and asymmetric vibrations of CH_2 and CH_3 groups [32] from the acidic protein matrix. The weak doublet seen at 2323 cm^{-1} is due to M–C=O coordination.

The moderately broad band that appeared at 1645 cm^{-1} with a halfwidth of approximately 100 cm^{-1} contains two bands, which are merged. It contains the amide I of the random coil protein [33]. The bands that observed between 1450 and 1650 cm^{-1} contains bands corresponding to the amide I and amide II of protein. Generally the bands corresponding to amide I are strong, amides II and III are weak. The bands observed between 1200 and 1350 cm^{-1} can be attributed to amide III arising from N–H deformation. The bands observed at 1027 and 1057 cm^{-1} are indicative of the presence of phosphate anion. The strong band observed at 1467 cm^{-1} and a shoulder on it in association with 842 and 739 cm^{-1} are characteristic bands of CO_3^{2-} ion.

4. Discussion

Earlier studies on XRD had noted the presence of calcium carbonate in other polymorphic forms, i.e., vaterite and aragonite in various combinations. However, from the present study, it is found that the primary constituent of the *pancreatic calculi* is calcium carbonate, in the form of calcite and peaks corresponding to aragonite have also been noticed and are indexed as per crystal phases of $CaCO_3$ in dimorphic form. However, the presence of calcium phosphates is also evidenced from the XRD, which is in confirmation with the

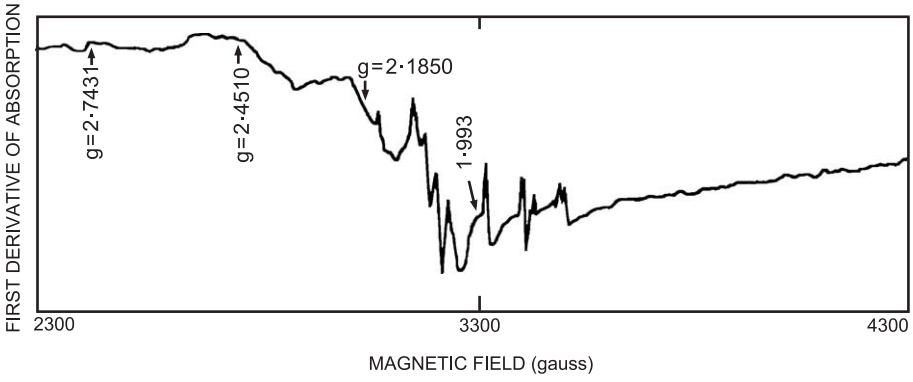

Fig. 6. EPR spectrum of the *P. calculi* sample recorded at 183 K showing resonances due to Mn^{2+} and Mn^{3+} as marked in the figure.

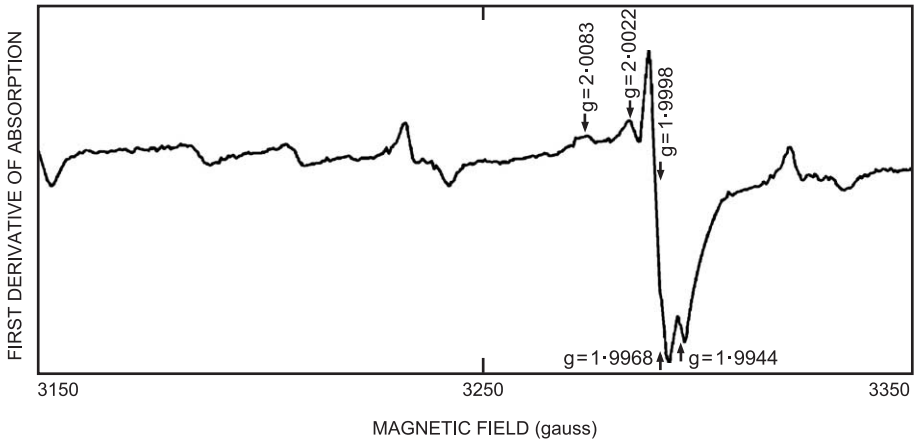

Fig. 7. EPR spectrum of X-irradiated *P. calculi* sample at room temperature. Note the changes in the spectrum in free radical region with number of resonance signals.

earlier studies [16,35]. The presence of aragonite peaks clearly demonstrates that, the soluble proteins may mediate the aragonite growth [17]. This is in good agreement with the arguments of De Reggi and Gharib [4] that the pancreatic stone protein may involve and mediate the stone formation. This would also support the conclusions drawn by Gerbaud et al. [15] that the lithostathine may modify the growth habit of the crystallization. The intense peak assigned with *hkl* (104) is indicative of the presence of calcite as the major phase present in the sample. Using the standard calibration methods of peaks C(104) and A(221) of calcite and aragonite, the relative molar fractions of calcite and aragonite phases were estimated according to the method described elsewhere [36]. Accordingly, the molar fraction of phosphate was also estimated. The relative concentrations of calcite, aragonite and calcium phosphate in this specimen are approximated to 59.14%, 35.7% and 5.14%, respectively.

The absence of any organic free radical signal in fresh *P. calculi* infers that the protein is strongly bound to Ca^{2+} ions in the calcite, referring to pancreatic stone protein binding at crystal faces of calcite. Usually, it happens by repulsive adsorption, thereon to incorporate into the crystal lattice in front faces during growth. The EPR spectra observed at room temperature (Fig. 1) clearly show that the Mn ions are present in divalent state. However, the presence of very weak Mn^{2+} signals can be either due to crystal strains present in the sample or may be due to their association with Mn^{3+} ions in a non-magnetic state, which is expected to be a natural impurity in all calcified materials or may be Mn^{3+}–Mn^{2+} in the form of redox couple similar to Mn-SOD [37]. Another possibility is that the Mn may strongly bind to the protein, which cannot be ruled out. The spectra observed at 200 and 400 °C rules out the possibility of any crystal strains. Hence, it may be expected that this material contain manganese in trivalent as well as divalent states. Hence, the sextet hyperfine spectrum observed at room temperature is due to Mn^{2+} ions. This can be confirmed in the EPR spectrum observed at low temperatures as given in Fig. 6, evidenced by additional resonances appeared at g=4.0570, 3.1970, 2.7431, 2.4510, 2.1850 which are not exactly due to Mn^{2+} ions, and may also be due to other oxidation states. Some of them (g=2.74, 2.1), are expected to be due to contributions from other fine structure transitions of Mn^{2+} (S=I=5/2), $|-5/2\rangle \rightarrow |-3/2\rangle$, $|-3/2\rangle \rightarrow |-1/2\rangle$ [38]. In the

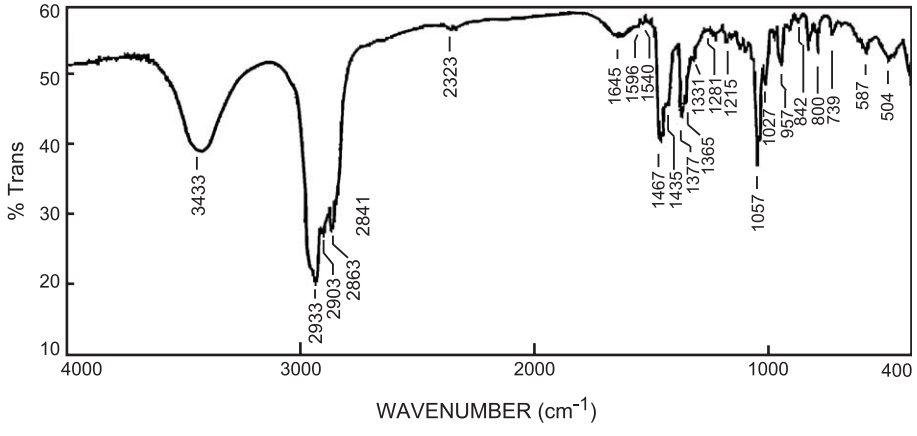

Fig. 8. The infrared spectrum of powdered *P. calculi* sample recorded at room temperature. The spectrum was measured in transmission mode using KBr Pellet technique.

process of sintering at relatively higher temperatures (>200 °C), the amide groups (protein matter) related to crystal composition may be lost due to decomposition of organic matter and hence, the study refers to $CaCO_3$ and its related components at high temperatures.

The sextet lines observed in the spectrum at room temperature, when the sample is heated at 200 °C are due to the allowed (ΔM_I=0) hyperfine lines. Between two consecutive hyperfine lines, there exist doublet lines of relatively less intensity, corresponding to forbidden transitions ($\Delta M_I \neq 0$). According to Bleaney and Rubins [35], these forbidden doublets are due to mixing of the hyperfine levels by the zero-field splitting parameter D. These forbidden lines can be assigned to $|1/2, M_I\rangle \leftrightarrow |-1/2, M_I-1\rangle$ and $|1/2, M_I-1\rangle \leftrightarrow |-1/2, M_I\rangle$ (M_I=5/2, 3/2, 1/2, −1/2, −3/2, −5/2) transitions. These forbidden transitions in polycrystalline samples produce valuable information regarding the symmetry environment, which indeed is helpful in our case in order to find the polymorphic forms of $CaCO_3$.

As seen in Fig. 3, the new sharp line appeared at g=2.0 is due to the CO_3^- radical formed during the thermal treatment [31], during which, liberation of CO_2 also takes place. The linewidth (8 G) and the evolution of this radical clearly indicate that this radical is due to the CO_3^- ion and is in good agreement with the earlier reports in literature [5,20,31], where the radical is found to appear at g=2.0113 (ΔB=4 G) [5] and g=2.0121 (5.5 G) [39]. Thus, the CO_3^- radical is formed due to the presence of PO_4^{3-} and CO_3^- anion impurities. Such evolution of the radical formation is possible when PO_4^{3-} ions in $CaCO_3$ would introduce neighboring charge compensator, i.e., an anion vacancy. The presence of the isotropic CO_3^- signal conceives the possibility of such phosphate impurities [24]. In the spectra recorded at higher temperatures, two more sets of sextet hyperfine lines have also been seen. This is possible when the PO_4^{3-} ions in $CaCO_3$ would introduce neighboring positively charged ion vacancy. The presence of PO_4^{3-} is highly possible in this material as can be seen in XRD and, hence, one can safely assume the generation of one more cation vacancy in which Mn^{2+} is situated. If it is true, at certain high temperatures, this vacancy may disappear at which $CaCO_3$ transforms to CaO, which agrees well with the EPR spectra observed at a sintering temperature of 700 °C. Though the samples are heated more than 700 °C, EPR spectral features are similar above this temperatures also (say above 800 °C), where the transformation of $CaCO_3$ to CaO may occur completely. Hence, we restrict our discussion up to 700 °C.

At relatively high temperatures, the sample shows a broad resonance signal centred at g=1.9983 with a linewidth of 10 G, which is entirely different from the CO_3^- radical observed earlier. This is attributed to Cr^{3+} isotopes (^{54}Cr, ^{52}Cr without any nuclear spin). Similar observations were reported in the case of a biomineralized marine shell valve where the proteins involve in biomineralization of the shell surface [20] and also in CaS material [40] containing manganese ions in traces. Such signal at g=1.9983 is in good agreement with those reported for Cr^{3+} in biological complex [41]. As is seen in Fig. 6, the ESR signals that appeared at resonances g=4.0570, 3.1970, 2.7431, 2.4510, 2.1850 can be attributed to the various oxidation states of manganese ions in low symmetry environments, normally observed at low temperatures [29,30]. This is quite possible in many biological systems [42], where Mn ions exist in different oxidation states, in the presence of effective coordination environments.

As seen in Fig. 7, the X-irradiated sample exhibits clear changes in the free radical region with a number of additional resonance signals centered at g=2.0083, 2.0022, 1.9998, 1.9968 and 1.9944. The resonances signals in Fig. 7 at g_{xx}=2.0022, g_{yy}=1.9998 and g_{zz}=1.9968 can be attributed to the g-values of orthorhombic CO_2^- radical ions. This agrees well with earlier results on the irradiated $CaCO_3$ materials [20,24,25]. Such signals in calcites have been attributed to be due to the freely rotating CO_2^- radical [24]. These signals have also been observed in $CaCO_3$ shells in aragonite symmetry [25], where there is no possibility of free rotation of CO_2^- radical due to the complex symmetry (due to lack of free space in the lattice) unlike the calcite dominant materials in the present work.

As can be seen in Fig. 4, the new resonance lines similar to ones observed for Mn^{2+}, but with different line widths (marked as Cr^{3+}) can be attributed to Cr^{3+} (^{53}Cr) with S=I=3/2. The additional lines present here are not due to manganese, but are due to the presence of one of the chromium isotopes in very rare cases [40,43]. It is well understood that Cr^{3+} is biologically active ion and acts as a cofactor for insulin. It appears to be required for carbohydrate and lipid metabolism in mammals [26] and plays an important role in lipid metabolism [25,27] in a variety of biochemical reactions and a novel biological role of chromium in regulation of insulin function is described elsewhere [25,44]. The main reason for the detection of Cr-related defect is given by the fact that the hyperfine structure reflects the natural abundance of isotopes. Cr is the only element having isotopes and fulfils the observed splitting. The central line at g=1.9983 is due to the isotopes ^{54}Cr, ^{52}Cr and ^{50}Cr without any nuclear spin, and the four line pattern indicated in Fig. 4, are due to the isotope ^{53}Cr having a nuclear spin I=3/2 with a natural abundance of 9.55% [40,43]. Such a Cr^{3+} ion is possible to occupy the substitutional cation site, which may be occupied from one of the Ca^{2+} sites, where it is being already occupied by Mn^{2+}. At high temperatures, the oxidation state of Cr is very much influenced such that the lattice energy may provide a chance for the lattice neutral Cr^{2+} ion states to change into the Cr^{3+} states, which is an EPR observable. The observed splitting of quartet hf lines (A=24 G) is in better agreement with that reported for Cr^{3+} ions in literature [40,43].

In the infrared spectrum of *P. calculi* shown in Fig. 7, the bands observed at 3433, 2933 and 2863 cm^{-1} correspond to

the protein material in the *P. calculi*. Though it contains larger proportions of calcified calculi, predominant presence of the protein amide bands were witnessed in the IR spectrum due to large acidophilic protein. This is in good agreement with the observations of pancreatic stone protein (lithostathine) with a 16 kDa length in calcified *pancreatic calculi* which is found in the case of the patients suffering from chronic pancreatitis [44]. These bands are similar to the IR results of gallstone protein reported by Kleiner et al. [45], they attributed these bands to the CH_2 and CH_3 bands corresponding to the pancreatic juice containing 16 kDa acidic protein. The infrared band positions and their assignments are clearly presented in Table 3. The broad band centered at 1645 cm^{-1} matches exactly with amide I [46] indicating the presence of low concentrations of protein in the calcified stones.

As said above, the amide bands of the random coil protein contains bands between 1650 and 1450 cm^{-1}, the bands appeared at 1200–1350 cm^{-1} correspond to the amide III of the protein present in the *P. calculi*. The band appeared as a shoulder at 1467 cm^{-1} is specifically, a characteristic doubly degenerate asymmetric stretching ν_3(E) band of CO_3^{2-} molecular ion, which appears due to the heavier calcification of the pancreatic stones. This indicates that, these stones are calcified and the protein bands are weakened. The band occurred at 1377 cm^{-1} with a sharp band at its shoulder is characteristic of carboxyl ions. This occurs normally due to the interaction of carboxyl groups with the metal ions [47]. This is also supported by the presence of weak doublet at 2323 cm^{-1} that, the metal ion is coordinated to carboxyl group (M–C=O), which cannot be seen in artificially synthesized $CaCO_3$ crystals [48] and hence the possibility of this band due to CO_2 can be ruled out in the present case. The bands at 957 cm^{-1} and the other at 1057 cm^{-1} are due to the $\nu_1(A_1)$ and ν_3(E) PO_4^{3-} molecular ion in a complex [34]. The band observed at 957 cm^{-1} is due to of PO_4^{3-}. The sharp band observed at 842 cm^{-1} is due to $\nu_2(A_2)$ of carbonate ion and the band at 800 cm^{-1} is due to –NH metal coordination. The weak band at 739 cm^{-1} can be assigned to the in-plane bending mode ν_4(E) of carbonate molecular ion. The band corresponding to ν_3(E) of CO_3^{2-} can be seen at 1435 cm^{-1}. The sharp band observed at 1027 cm^{-1} particularly arises due to aragonitic symmetry of calcium carbonate. The bands observed at 587 and 504 cm^{-1} are due to ν_4(E) of phosphate and NH_2 twist, respectively. The presence of aragonite phases in these stones may well be documented with the inception that the aragonite material will influence the calcification, hardening processes of the stones and further, this also influences the calcium phosphate formation [49]. Also, the higher calcification indicates the lesser amounts of lithostathine secretion, which indeed is observed in our detailed experiments. Such higher calcification indicates the increasing attitude of chronic pancreatitis disease.

Table 3
The infrared band positions and their tentative assignments in the case of *P. calculi* samples

Band position	Assignment	
3433 (s, vb)	–OH	protein β sheet
3063 (w)	–NH	H-bonded
2933 (m, s)	C–H	assymmetric stretch
2903 (m)	C–H	
2863, 2841… (sh, triplet)	C–H	symmetric stretch
2323 (doublet)	M–C=O	metal coordination
1645 w	–C=O	amide I
1596 w	C=O stretch	ν_{as}
1540 (vw)	COO^- antisymmetric stretch	amide II
1467 (m)	C–H	CH_2 bend
1435 (w, sh)	ν_3(E) assymmetric stretch	CO_3^{2-}
1377	C–OH	
1365 (m)		
1331	N–H deform	amide III
1281 (vw)		
1215 (vw)	C=O	stretch
1057 (sp)	ν_3(E)	PO_4^{3-}
1027 (sh)	CO_3^{2-}	aragonite
957	$\nu_1(A_1)$	PO_4^{3-}
842 (sp)	$\nu_2(A_2)$	CO_3^{2-}
800 (sp)	–NH	M–N coordination
739 w	ν_4(E)	CO_3^{2-}
587 w	ν_4(E)	PO_4^{3-}
504	N–H	N–H twist

s=strong, w=weak, m=medium, sp=sharp, sh=shoulder, vb=very broad, vw=very weak, M=metal ion.

5. Conclusions

The pancreatic stones collected from the patients suffering from chronic pancreatitis have been studied by XRD, EPR and infrared spectra. From the XRD studies, it is found that the primary constituent of the *pancreatic calculi* is calcium carbonate, in the form of calcite (major), aragonite and the tracer amounts of phosphates. The presence of aragonite peaks here demonstrates the involvement of protein macromolecules in calcification process. The biomineralized species of the pancreatic stones were explored with thermal sintering and also with the X-irradiation experiments, using EPR technique. This technique has also been utilized taking the advantage of the presence of paramagnetic manganese ions in traces. The detailed spectral studies demonstrate the possibility of two or more salts of calcium in the calcified samples. We have explored the dynamics of the carbonate radical species in the form of CO_3^- and CO_2^- molecules using the thermal and X-irradiation assisted by EPR technique. The infrared spectrum observed at room temperature shows number of bands characteristic of calcium carbonate and the calcium binding protein in the complex. The detailed experiments conclude that, the lithostathine would involve in the pancreatic stone formation.

Acknowledgement

The authors are very thankful to Prof. Lian-Pin Hwang, Department of Chemistry, National Taiwan University, Taipei for many suggestions in this work.

References

[1] H.G. Beger, A.L. Warshaw, D.L. Carr-Locke, J.P. Neoptolemos, C. Russell, M.G. Sarr, The Pancreas, Blackwell Scientific Publications, London, 1998.

[2] J. Geevarghese, Calcific Pancreatitis: Causes and Mechanisms in the Tropics Compared in the Subtropics: I, Varghese Publishing House, Bombay, 1976.

[3] C. Cerini, V. Peyrot, C. Garnier, L. Duplan, S. Veesler, Le Caer, J.P. Bernard, H. Bouteille, R. Michael, A. Vazi, P. Dupuy, B. Michael, Y. Berland, J.M. Verdier, Biophysical characterization of lithostathine: evidences for a polymeric structure at physiological p^H and a proteolysis mechanism leading to the formation of fibrils, J. Biol. Chem. 274 (1999) 22266–22274.

[4] M. De Reggi, B. Gharib, Protein-X, pancreatic stone-, pancreatic thread-, reg-protein, P19, lithostathine, and now what? Characterization, structural analysis and putative function(s) of the major non-enzymatic protein of pancreatic secretions, Curr. Protein Pept. Sci. 2 (2001) 19–42.

[5] V. Mohan, S.J. Nagalotimath, C.S. Yajnik, B.B. Tripathy, Fibrocalculous pancreatic diabetes, Diabetes Metab. Rev. 14 (1998) 153–170.

[6] V. Mohan, C.S. Pitchumoni, Tropical chronic pancreatitis, in: H.G Begerm, A.L Warshaw, D.L Carr-Locke, J.P Neoptolemos, C. Russell, M.G. Sarr (Eds.), The Pancreas, Blackwell Scientific Publications, London, 1998, p. 688–697.

[7] A.C. Schulz, P.B. Moore, P.J. Geevarghese, C.S. Pitchumoni, X-ray diffraction studies of *pancreatic calculi* associated with nutritional pancreatitis, Dig. Dis. Sci. 31 (1986) 476–480.

[8] D. Mustafi, B.-I. Lee, A. Sosa-Peinado, Y. Nakagawa, W. Cho, Calcium-binding properties of an important calcite growth inhibitor protein: lithostathine, Biochemistry 40 (2001) 205.

[9] R. Abe, T. Shimosegawa, S. Moriizumi, Y. Kikuchi, K. Kimura, A. Satoh, M. Koizumi, T. Toyota, Lipopolysaccharide induces manganese superoxide dismutase in the rat pancreas: its role in caerulein pancreatitis, Biochem. Biophys. Res. Commun. 217 (1995) 1216–1222.

[10] J.J. Cullen, F.A. Mitros, L.W. Oberley, Expression of antioxidant enzymes in diseases of the human pancreas: another link between chronic pancreatitis and pancreatic cancer, Pancreas 26 (2003) 23–27.

[11] H. Jouve, H. Jouve, E. Melgar, B. Lizarraga, A study of the binding of Mn^{2+} to bovine pancreatic deoxyribonuclease I and to deoxyribonucleic acid by electron paramagnetic resonance, J. Biol. Chem. 250 (1975) 6631–6635.

[12] V.M. Marathias, K.Y. Wang, S. Kumar, T.Q. Pham, S. Swaminathan, P.H. Bolton, Determination of the number and location of the manganese binding sites of DNA quadruplexes in solution by EPR and NMR in the presence and absence of thrombin, J. Mol. Biol. 260 (1996) 378–394.

[13] B.-I. Lee, D. Mustafi, W. Cho, Y. Nakagawa, Characterization of calcium binding properties of lithostathine, J. Biol. Inorg. Chem. 8 (2003) 341–347.

[14] P. Merdy, E. Guillon, M. Aplincourt, Iron and manganese surface complex formation with extracted lignin: Part 1. Adsorption isotherm experiments and EPR spectroscopy analysis, New J. Chem. 26 (2003) 1638–1645.

[15] V. Gerbaud, D. Pignol, E. Loret, J.A. Bertrand, Y. Berland, J.C. Fontecilla-Camps, J.P. Canselier, N. Gabas, J.M. Verdier, Mechanism of calcite crystal growth inhibition by the N-terminal undecapeptide of lithostathine, J. Biol. Chem. 275 (2000) 1057–1064.

[16] M. Sivakumar, T.S. Sampath Kumar, K.L. Shantha, K.P. Rao, Development of hydroxyapatite derived from Indian coral, Biomaterials 17 (1996) 1709–1714.

[17] Q.L. Feng, Z.Z. Cui, G. Pu, R.Z. Wang, H.D. Li, Crystal orientation, toughening mechanisms and a mimic of nacre, Mater. Sci. Eng., C, Biomim. Mater., Sens. Syst. 11 (2000) 19–25.

[18] W. Low, S. Zeira, ESR spectra of Mn^{2+} in heat-treated aragonite, Am. Mineral. 57 (1972) 1115–1124.

[19] K.V. Narasimhulu, J. Lakshmana Rao, EPR and IR spectral studies of the sea water mussel *Mytilus conradinus* shells, Spectrochim. Acta, A Mol. Spectrosc. 56 (2000) 1345–1353.

[20] C.P. Lakshmi Prasuna, K.V. Narasimhulu, N.O. Gopal, J.L. Rao, T.V.R.K. Rao, The microstructures of biomineralized surfaces: a spectroscopic study on the exoskeletons of fresh water (apple) snail, *Pila globosa*, Spectrochim. Acta, A Mol. Spectrosc. 60 (2004) 2305–2314;
C.L. Raju, K.V. Narasimhulu, N.O. Gopal, J.L. Rao, B.C.V. Reddy, Electron paramagnetic resonance, optical and infrared spectral studies on the marine mussel *Arca burnesi* shells, J. Mol. Struct. 608 (2002) 201–211.

[21] A. Abragam, B. Bleaney, Electron Paramagnetic Resonance of Transition Ions, Oxford, London, 1970, p. 187.

[22] J.M. Nedelec, M. Bouazaoui, S. Turrel, Densification of Mn^{2+} doped monoclinic silica xerogels: an electron spin resonance study, Phys. Chem. Glasses 40 (1999) 264–268.

[23] W.C. Tennant, Forbidden lines in ESR of Mn^{2+} in calcite, J. Magn. Reson. 14 (1974) 152–159.

[24] S. Idrissi, F. Callens, P. Moens, R. Debuyst, F. Dejehet, An electron nuclear double resonance and electron spin resonance study of isotropic CO_2^- and SO_2^- radicals in natural carbonates, Jpn. J. Appl. Phys. 35 (1996) 5331–5332.

[25] S.S. Ishchenko, I.P. Vorona, S.M. Okulov, N.P. Baran, C-13 hyperfine interactions of CO^{2-} in irradiated tooth enamel as studied by EPR, Appl. Radiat. Isotopes 56 (2002) 815–819.

[26] H.C. Lukaski, Chromium as a supplement, Annu. Rev. Nutr. 19 (1999) 279–302.

[27] J.B. Vincent, Recent advances in the nutritional biochemistry of trivalent chromium, Proc. Nutr. Soc. 63 (2004) 41–47.

[28] R. Stoyanova, M. Gorova, E. Zhecheva, EPR of Mn^{4+} in spinels $Li_{1+x}Mn_{2-x}O_4$ with $0 \le x \le 01$, J. Phys. Chem. Solids 61 (2000) 609–614.

[29] D. Ramirez-Rosales, R. Zamorano-ulloa, O. Perez-Martinez, Electron spin resonance study of the conversion of Mn^{4+} to Mn^{2+} in the $Pb_{1-x}Eu_xTi_{1-y}Mn_yO_3$ ceramic system, Solid State Commun. 118 (2001) 371–376.

[30] C.B. Azzoni, M.C. Mozzati, P. Ghigna, L. Malavasi, G. Flor, Magnetic investigations of Mn ions in $(Cd_{1-x}Mn_x)Mn_2O_4$ spinels, Solid State Commun. 117 (2001) 511–515.

[31] J.F. de Lima, M.E.G. Valerio, E. Okuno, Thermally assisted tunneling: an alternative model for the thermoluminescence process in calcite, Phys. Rev., B 64 (2001) 1–6 (art. no. 014105).

[32] M.C. Chang, J. Tanaka, FT-IR study for hydroxyapatite/collagen nanocomposite cross-linked by glutaraldehyde, Biomaterials 23 (2002) 4811–4818.

[33] S. Yoshida, T. Yubisui, K. Shirabe, M. Takeshita, Fourier transform infrared spectroscopies of protein structures of soluble NADH-cytochrome *b*(5) reductases prepared by site-directed mutagenesis: comparison with ferredoxin-NADP(+) reductase, Biospectroscopy 3 (1997) 215–223.

[34] P.B. Messersmith, S. Vallabhaneni, V. Nguyen, Preparation of calcium loaded liposomes and their use in calcium phosphate formation, Chem. Mater. 10 (1998) 109–116.

[35] B. Bleaney, R.S. Rubins, Explanation of some "forbidden" transitions in paramagnetic resonance (EPR), Proc. Phys. Soc. Lond. 77 (1961) 103–112.

[36] C.G. Kontoyannis, N.V. Vagenas, Calcium carbonate phase analysis using XRD and FT Raman spectroscopy, Analyst 125 (2000) 251–255.

[37] J.W. Whittaker, Manganese superoxide dismutase, in: A. Sigel, H. Sigel (Eds.), Metal Ions in Biological Systems; Manganese and Its Biological Processes, vol. 37, Marcell Decker, New York, 2000.
[38] S. Un, L.C. Tabares, N. Cortez, B.Y. Hiraoka, F. Yamakura, Manganese(II) zerofield interaction in cambialistic and manganese SOD, and its relationship to the structure of metal binding site, J. Am. Chem. Soc. 126 (2004) 2720–2726.
[39] I.C. Hisatsune, T. Adl, E.C. Beahm, R.J. Kempf, Matrix isolation and decay kinetics of carbon dioxide and carbonate anion free radicals, J. Phys. Chem. 74 (1970) 3225–3231.
[40] D. Gourier, D.D. Simons, D. Vivien, N. Ruelle, M. Pham Thi, Multiple-quantum EPR transitions of Mn^{II} in CaS: Mn^{II} phosphor, Phys. Status Solidi, B Basic Res. 180 (1993) 223–235.
[41] M. Kim, T. Okajima, S. Kishishita, M. Yoshimura, A. Kawamori, K. Tanizawa, H. Yamaguchi, X-ray snapshots of quinone cofactor biogenesis in bacterial copper amine oxidase, Nat. Struct. Biol. 9 (2002) 591–596.
[42] C.G. Chen, J. Kazimir, G.M. Cheniae, Calcium modulates photo-assembly of photosystem II Mn^{4+} clusters by preventing ligation of non-functioning high valency states of manganese, Biochemistry 34 (1995) 13511–13526.
[43] J. Kreissl, U. Troppenz, B. Huttl, L. Schrottke, C. Fouassier, Electron paramagnetic resonance and photoluminescence studies of chromium in SrS, Appl. Phys. Lett. 72 (1998) 1232–1234.
[44] C.X. Jin, S. Naruse, M. Kitagawa, H. Ishiguro, T. Kondo, S. Hayakawa, T. Hayakawa, Pancreatic stone protein of *pancreatic calculi* in chronic calcified pancreatitis in man, JOP. J. Pancreas 3 (2002) 54–61.
[45] O. Kleiner, J. Ramesh, M. Huleihel, B. Cohen, K. Kantarovich, C. Levi, B. Polyak, R.S. Marks, J. Mordehai, Z. Cohen, S. Mordechai, A comparative study of gallstones from children and adults using FTIR spectroscopy and fluorescence microscopy, BMC Gastroenterol. 2 (2002) 1–14.
[46] P. Bour, T.A. Keiderling, Emperical modeling of the peptide amide I band IR intensity in water solution, J. Chem. Phys. 119 (2003) 11253–11262.
[47] K. Nakamoto, Infrared Spectra of Inorganic and Coordination Compounds, Wiley, New York, 1963.
[48] L. Yang, X. Zhang, Z. Liao, Y. Guo, Z. Hu, Y. Cao, Interfacial recognition between polysaccharides and calcium carbonate during crystallization, J. Inorg. Biochem. 97 (2003) 377–383.
[49] L. Addadi, S. Raz, S. Weiner, Taking advantage of disorder: amorphous calcium carbonate and its roles in biomineralization, Adv. Mater. 15 (2003) 959–970.